Finite element analysis and experimental study of surface acoustic wave propagation through two-dimensional pillar-based surface phononic crystal

S. Yankin, Abdelkrim Talbi, Y. Du, Jean-Claude Gerbedoen, Vladimir Preobrazhensky, Philippe Pernod, Olivier Bou Matar

Journal of Applied Physics

Finite element analysis and experimental study of surface acoustic wave propagation through two-dimensional pillar-based surface phononic crystal

Cite as: J. Appl. Phys. **115**, 244508 (2014); https://doi.org/10.1063/1.4885460
Submitted: 23 April 2014 • Accepted: 15 June 2014 • Published Online: 26 June 2014

S. Yankin, A. Talbi, Y. Du, et al.

Finite element analysis and experimental study of surface acoustic wave propagation through two-dimensional pillar-based surface phononic crystal

S. Yankin,[1,2,a)] A. Talbi,[1] Y. Du,[1] J.-C. Gerbedoen,[1] V. Preobrazhensky,[1,3] P. Pernod,[1] and O. Bou Matar[1]

[1]*International Associated Laboratory LICS/LEMAC: IEMN, UMR CNRS 8520, PRES Lille Nord de France, EC Lille, 59652 Villeneuve d'Ascq, France*

[2]*Saratov State University, Astrakhanskaya Str. 83, 410012 Saratov, Russia*

[3]*International Associated Laboratory LICS/LEMAC: Wave Research Center, GPI RAS, 38 Vavilov Str., 119991 Moscow, Russia*

(Received 23 April 2014; accepted 15 June 2014; published online 26 June 2014)

We study both theoretically and experimentally the interaction of surface elastic waves with 2D surface phononic crystal (PnC) on a piezoelectric substrate. A rigorous analysis based on 3D finite element method is conducted to calculate the band structure of the PnC and to analyze the transmission spectrum (module and phase). Interdigital transducers (IDTs) are considered for electrical excitation and detection, and absorbing boundary conditions are used to suppress wave's reflection from the edges. The PnCs are composed of an array of 20 Nickel cylindrical pillars arranged in a square lattice symmetry, and deposited on a $LiNbO_3$ substrate (128°Y cut-X propagating) between two dispersive IDTs. We investigate by means of band diagrams and transmission spectrum the opening band-gaps originating from pillars resonant modes and from Bragg band-gap. The physical parameters that influence and determine their appearance are also discussed. Experimental validation is achieved through electrical measurement of the transmission characteristics, including amplitude and phase. © *2014 AIP Publishing LLC*.
[http://dx.doi.org/10.1063/1.4885460]

I. INTRODUCTION

Phononic crystals (PnCs) are created by periodic arrays (1D, 2D, 3D) of elastic structures displaying a strong contrast in their elastic properties and densities. The ability to control the propagation of elastic waves with such composite materials has attracted a considerable attention during the last two decades from science and technology points of view.[1,2] The interest in PnCs is linked to their unique properties, such as the formation of band-gaps,[3,4] near zero group velocity,[5] and anomalous dispersion (negative refraction),[6] similar to the ones of photonic crystals.[7] The targeted applications depend on the PnC operation frequency. For example, sonic PnCs are important for sound manipulation,[8] and ultrasonic PnCs play a role in imaging, non destructive testing, and communication.[2] Finally hypersonic PnCs may lead to new applications, including microwaves and multi-physics signal processing (optic, magnetic, thermoelectric).[9,10] In the microwave domain, such PnCs unique properties can be investigated and exploited in the best way, in designing practical devices like high quality factor resonators,[11] novel transducers[1,2,12] and in implementation of such electronic functions as filtering, guiding, focusing, or demultiplexing.[13–16]

Various research groups have focused their interest on different configurations of PnCs constituted from solid, liquid, or air scattering inclusions in a solid background, and vertical pillars or line trench on top of a substrate[2] or plate.[17–19] The 2D surface PnC is gaining more and more research interest because of compatibility with standard micro-machining process and because of the ability to provide complex elastic waves processing. This will enable to open new perspectives[1] in designing high performance acoustoelectronic devices, e.g., resonators, pass-band, and low-band filters.

During last few years, numerous publications related to the usage of piezoelectric materials for excitation and detection of surface acoustic wave (SAW) or Lamb wave propagation through PnCs appeared. Among them there are various theoretical and experimental reports on the existence of band-gaps in a square lattice of air holes in $LiNbO_3$[20,21] and in lattice of pillars deposited on the surface of a $LiNbO_3$ substrate.[22–24] Other studies have been devoted to the physical principles underlying the forbidden zones creation in ZnO and AlN plates using different topologies of PnC.[25–28]

Nowadays, one of the main aspects in the theoretical studies of PnC is the analysis of the dispersion characteristics of ideal infinite PnC lattices to calculate the frequency dependence of the acoustic modes from the wave vector within the first Brillouin zone, and to determine bandwidths and stop-bands of various PnC topologies. In the case of two-dimensional phononic crystals in the form of cylindrical pillars on a piezoelectric substrate, calculations using the finite element (FE) method show the existence of various opening band-gaps for surface acoustic waves created by local resonant state of PnC elements and Bragg scattering.[22] Furthermore, the analysis used in this reference provides information about the elastic wave modes localized in the PnC but situated above the branch corresponding to the lower bulk transverse modes with different longitudinal or transverse polarization.

a)Electronic mail: sergey.farsenal@gmail.com.

Another proposed approach is to calculate the transmission through realistic structure using either analytical[29] or FE methods[22] that can give not only qualitative but also quantitative characteristics of the wave transmission. In all mentioned works, the SAW excitation was performed using harmonic force source with specified polarization direction excluding the impact of interdigital transducers (IDTs) on the amplitude-phase characteristics. This point is of a great interest and taking it into account can improve the design of microwave acoustoelectronic devices.

The main objective of this study is the analysis of SAW transmission characteristics through PnC considering the piezoelectric properties of the substrate and the influence of IDTs. In this paper, we numerically investigate SAW band gap formation in a periodic array of cylindrical nickel pillars on a 128°Y cut-X propagating $LiNbO_3$ piezoelectric wafer, and compare calculation results with experimental data.

This paper is organized as follows. In Sec. II, we present the model and methods for computing the SAW band diagrams and electrical transmission spectra, i.e., SAW generation and detection. In Sec. III, the numerical results are presented and discussed. In Sec. IV, we present an experimental validation of the obtained theoretical results. Finally, in Sec. V, we summarize the main results.

II. MODEL DESCRIPTION

To model PnC structures made of cylindrical pillars deposited on a piezoelectric substrate, we use the commercial FE software COMSOL Multiphysics.[30] This software allows us to simulate the propagation of acoustic waves in complex structures, including piezoelectric effects in the substrate.

The band diagram of the perfect 2D surface PnC is calculated using the eigenfrequency solver of the general partial differential equations (PDE) module. We consider the unit cell of the 2D PnC, as shown in Fig. 1(a). It is composed of a cylindrical nickel pillar deposited on the piezoelectric substrate's surface. A commonly used 128°Y cut-X propagating $LiNbO_3$ is chosen as piezoelectric substrate. All typical geometry sizes are displayed on the schematic drawing (Fig. 1(a)): a, h, and r refer to the lattice constant, pillar thickness, and pillar radius, respectively. Periodic boundary conditions of Bloch-Floquet type are applied along the X and Y directions, i.e., the lateral sides of the unit cell, to represent an infinite PnC structure. In this way, eigenfrequency problem of such system was solved during parametric sweep of the wave vector in the first Brillouin zone (Fig. 2). Obtained values of eigenfrequencies, corresponding to different acoustic modes excited in such periodic array, are then analyzed and represented as function of the reduced wave vector in the form of a band diagram.

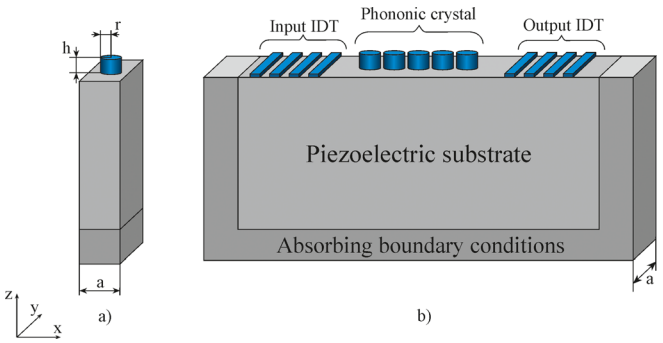

FIG. 1. (a) Model of unit cell of the square periodic pillar based structure; the lattice parameter is denoted as a, the height of the stub is denoted as h, and the radius is denoted as r and (b) model of device used for the calculation of SAW transmission through PnC.

It should be noted that in this study, we principally focus on the surface modes. For that aim, absorbing boundary layers are applied to the bottom, instead of using high bulk velocity substrate like silicon, as used in most of the previous works.[22,23] Such method also helps to suppress wave reflections from the bottom.

For transmission spectra calculations, we consider a SAW device composed of two dispersive IDTs, and a PnC placed between them. The model is depicted on Fig. 1(b). It assumes PnC with finite size (here an array of 20 pillars) along the wave propagation direction (X). At the same time, width of the model in the Y direction is equal to the PnC period a. On the sidewalls, in this direction, periodic boundary conditions are applied. They allow us to consider a PnC of infinite size in the Y direction. The dispersive aluminum IDTs are designed to cover a wide frequency range, providing the observation of all potential band gaps. The piezoelectric substrate is surrounded by layers with absorption chosen in order to suppress undesired reflections from boundaries. The incident waves are excited by applying a harmonic voltage (amplitude close to 1 V) to the input IDT used as emitter. The transmitted waves are detected by measuring the voltage (amplitude and phase) on a similar output IDT, used as a receiver. This allows evaluating the transmission spectrum of the electric signal that passed through PnC in a similar manner as the one used to measure the S_{21} element of the scattering matrix. Comparing this data with reference delay line characteristics without PnC, S_{21ref}, one can calculate the relative transmission dependence ΔS_{21}, and the accumulation of phase difference $\Delta\varphi$

$$\Delta S_{21} = |S_{21ref}| - |S_{21}|, \tag{1}$$

$$\Delta\varphi = Arg(S_{21}) - Arg(S_{21ref}). \tag{2}$$

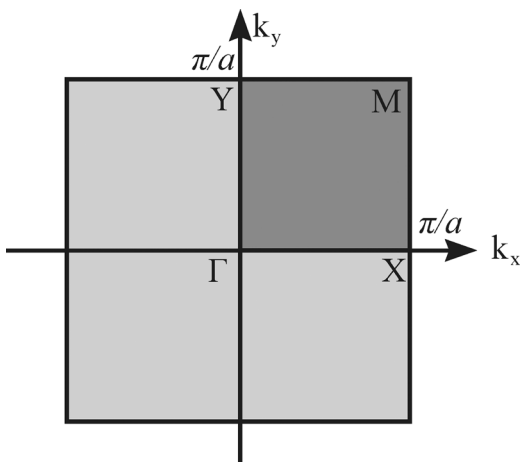

FIG. 2. The first Brillouin zone for the reduced wave vector.

III. SIMULATION RESULTS

The interaction of acoustic waves with PnC made of pillar deposited on a substrate, as shown in Ref. 22, leads for certain parameters of the crystal to the appearance of two stopbands in the frequency spectrum, the first of which is caused by the combined resonances of scattering inclusions (in this case pillars) of the PnC, and the second is related to Bragg scattering. Bragg scattering occurs when the wave vector k of the incident wave tends to the edge of a Brillouin zone. The central frequency of Bragg gap can only be tuned by the period of the structure or by the wave velocity in the material under PnCs. On the other hand, the first band-gap exists only if the scattering objects have strong resonances in the frequency range of interest. The underlying physical principle is based on the excitation of pillars discrete resonant modes, including bending, compressive, and shear modes. Therefore, these band gaps will depend on the pillars geometrical parameters, including shape, thickness, and radius. So, in order to limit the range of different geometrical parameters, the structures investigated in this study are chosen with a fixed lattice constant ($a = 10\,\mu$m) and a fixed filling factor ($r = 3.8\,\mu$m). We only consider the effect of pillars thickness on the band structure. Two different values are assumed: (a) $h = 2.3\,\mu$m and (b) $h = 3.4\,\mu$m.

Let us consider the dispersion characteristics for the two parameter sets. The corresponding band diagrams are displayed in Fig. 3. Note that the gray color on the graphs denotes the radiation zone, i.e., zone of bulk mode excitation,[1,2] for the crystal $LiNbO_3$. Surface modes interesting for this study lie outside the radiation zone, below the sound cone curve (bold solid line) corresponding to the Rayleigh SAW in the absence of a periodic structure.

For $h = 2.3\,\mu$m, as we can notice from Fig. 3(a), considering PnC symmetry and anisotropy of $LiNbO_3$ crystal an opening full band-gap appears around 153 MHz with a width close to 5%. As can be seen from Fig. 4, which shows the shape of the acoustic modes corresponding to wave vectors at the point X, the first and third modes are polarized in the XZ plane, and modes 2 and 4 in the YZ plane. In the case of a 128°YX cut $LiNbO_3$ substrate, surface acoustic waves possess a pure sagittal polarization. So, if only SAWs are taken in account, then the local band gap emerges after 134 MHz. The second band gap, appearing near 176 MHz, corresponds to Bragg scattering. Furthermore, interaction of wave and PnC in the frequency range above 198 MHz would lead to bulk scattering.

In the case of $h = 3.4\,\mu$m, displayed in Fig. 3(b), we observe the existence of two complete band gaps. The first band gap appears around 135 MHz with width close to 33%. The second one appears around 195 MHz. If we take into consideration only the SAW propagating in the direction of X, then the first band gap begins above 108 MHz, and the second above 165 MHz.

From the two band diagrams, one can notice that the growth of the pillar's thickness leads to a decrease in the frequency at which the surface modes are excited in the system. This is due to the well-known effect of reduction of the velocity of SAW under a metal layer in a piezoelectric wafer.[31] With regard to the propagation of acoustic waves polarized in the sagittal plane, this leads to a significant decrease in the first band center frequency. Furthermore, the increase in the pillar's thickness induces the apparition of the second gap,[22] with a center frequency practically not shifted, but with an increasing width.

Let us now consider the quantitative characteristics of the SAW interaction with PnC structure. We collect during the calculation of the transmission spectra the relative transmission dependence and the accumulation of phase difference for the abovementioned two sets of parameters, as shown in Fig. 5.

As it is seen from the ΔS_{21} graph, for the first set of parameters, the local gap begins at 133 MHz and leads to about 40 dB of losses. It is important to note that the local maximum and minimum at 133 MHz and 135 MHz, respectively, correspond to resonance and antiresonance of the pillar's array. The Bragg gap appears after 175 MHz and the losses in that case are around 50 dB. It is interesting to compare the amplitude and phase characteristics of the transmission. Large growth of the phase difference is clearly visible near 133 MHz that corresponds to the start of the first forbidden zone. Local maximums around 134 and 175 MHz indicate that the group velocity of SAW shifts to zero, which is also evident from the band diagrams in Fig. 3. Furthermore, inside the bandgaps the phase difference stops to rise and remains almost constant. Elastic displacement distribution in the delay line, displayed in Fig. 6, illustrates the interaction

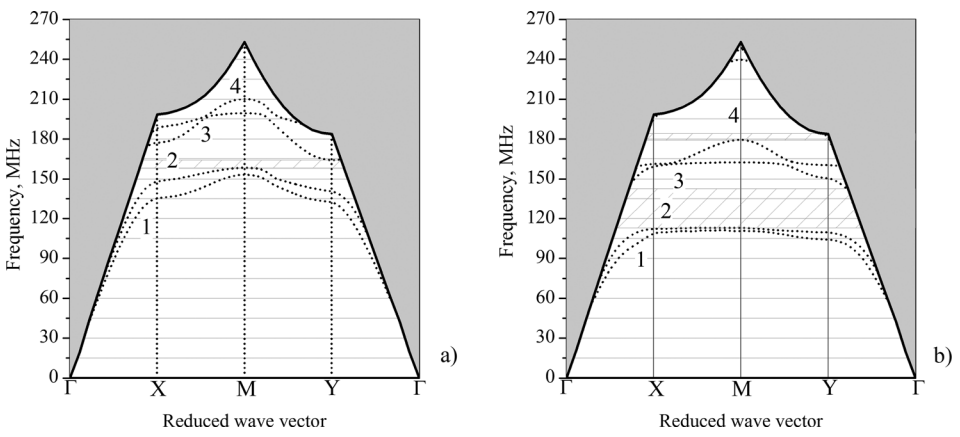

FIG. 3. Band diagrams for infinite PnC with lattice parameter $a = 10\,\mu$m, radius $r = 3.8\,\mu$m, and height (a) $h = 2.3\,\mu$m; (b) $h = 3.4\,\mu$m. Digits 1–4 indicate the number of the acoustic modes displayed in Fig. 4.

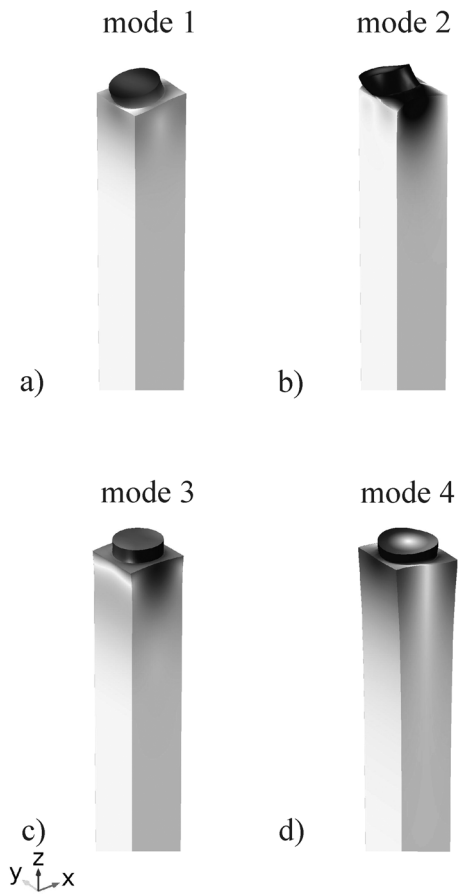

FIG. 4. Shapes of elastic deformations for the first four acoustic modes of the PnC described in Fig. 3. Gray gradient denotes the amplitude of deformation, where white color corresponds to its minimum, and black to the maximum.

of SAW on characteristic frequencies: $f = 100$ MHz, 133 MHz, 137 MHz, and 179 MHz. Fig. 6(a) corresponds to the $f = 100$ MHz inside the transmission frequency range and illustrates that SAW converts into Mode 1 (Fig. 4(a)) during propagation in the PnC. Fig. 6(b) demonstrates the pattern of elastic displacement that formed in the pillar's array at the local resonance frequency. Figs. 6(c) and 6(d) show the difference between first and second bandgap: for $f = 179$ MHz, in the Bragg band gap, we see that SAW is almost totally reflected from the PnC which acts like Bragg mirror (displacements after the fifth row of pillars are almost negligible), while for the case of $f = 133$ MHz, it is visible that the wave is gradually decrease along the pillar array.

Transmission spectrum (Fig. 5(b)) for the second parameter set shows that the band gaps are located where they are predicted by the dispersion characteristics (Fig. 3(b)). First band gap is observed at frequencies between 108 and 140 MHz, and Bragg band gap starts around 161 MHz. Clearly, for a given set of parameters, the two stop bands are well separated, i.e., at least 20 MHz of separation. The behavior of the phase difference becomes more complex than for the first case. It increases in the frequency range between the two observed gaps. This is in perfect agreement with the band diagram displayed in Fig. 3(b), where one can clearly observe that the third mode is not flat in the first Brillouin zone, contrary to the case where the pillar's thickness is small.

IV. EXPERIMENTAL RESULTS

For the experimental investigation, several samples with delay lines and PnC were fabricated. A $LiNbO_3$ Y-128°-cut wafer was used to favorize the generation of sagittal Rayleigh wave mode. To fabricate the IDTs, we start by the deposition of a 200 nm aluminum thin film by sputtering, followed by a standard lithography process to form the transducers. The IDTs exhibit a linear variation of the period along their length, from 4 μm to 40 μm. This design permits to cover the entire frequency range of interest, i.e., from 90 MHz to 250 MHz, so enabling an easy observation of band-gaps for the designed PnC. Nickel thin films with various thicknesses (2.3 μm and 3.4 μm) are electroplated inside a photoresist mould (AZ 15nXT) to obtain the desired square lattice of pillars. Scanning Electron Microscopy (SEM) images of one of the fabricated device are displayed in Fig. 7. The PnC is composed of 20 periods of a square lattice of pillars with a period of 10 μm. Two devices were fabricated with PnCs geometrical parameters as close as possible to the ones assumed in the numerical simulations.

The obtained PnCs are then characterized by measuring the scattering matrix (S_{ij}) with an Agilent Network analyzer 8753ES. After a standard short-open-load-through

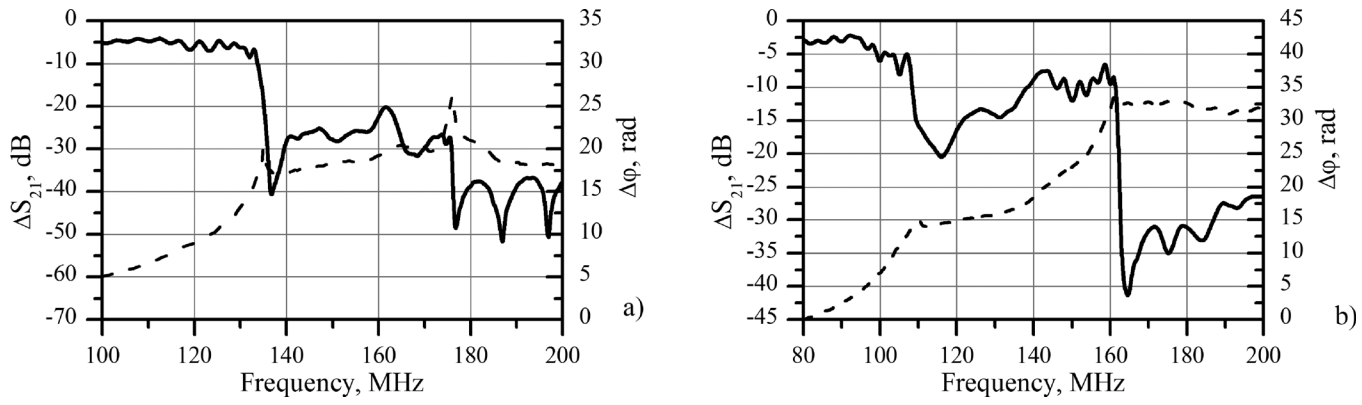

FIG. 5. Calculated frequency dependence of relative transmission ΔS_{21} (solid line) and accumulation of phase difference $\Delta\varphi$ (dashed line) for PnC made from $N = 20$ nickel pillars with lattice parameter $a = 10$ μm, radius $r = 3.8$ μm and height (a) $h = 2.3$ μm; (b) $h = 3.4$ μm.

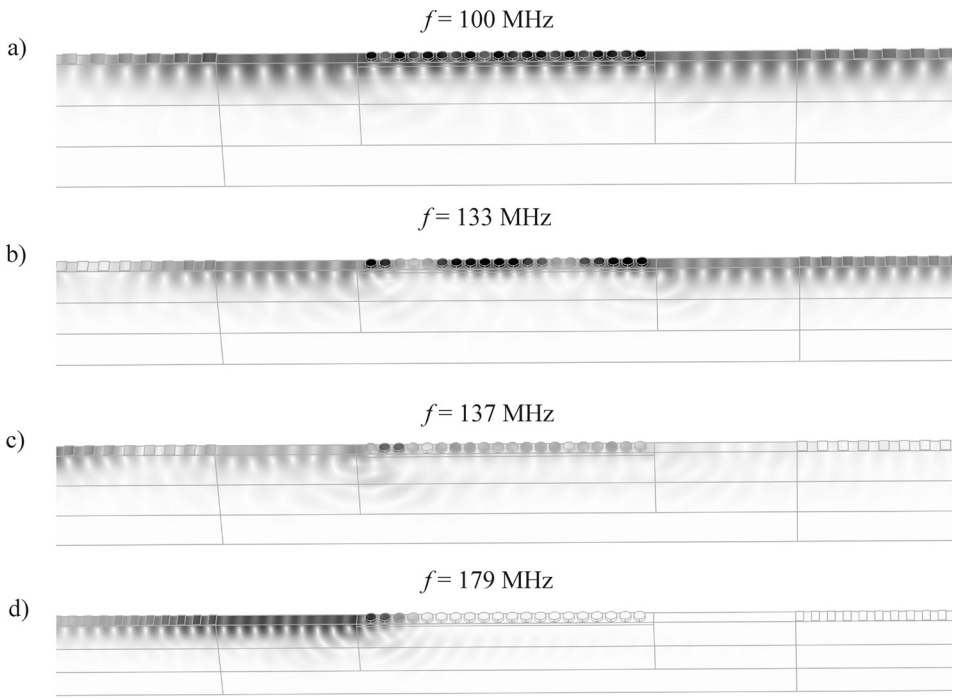

FIG. 6. Elastic displacement distribution in the delay line for characteristic frequencies: (a) $f = 100$ MHz—in the transmission frequency range, (b) $f = 133$ MHz—the 1st resonance of the pillars, (c) $f = 137$ MHz—in the first band gap, and (d) $f = 179$ MHz—in the Bragg band gap. Gray gradient denotes the amplitude of deformation, where white color corresponds to its minimum, and black to the maximum.

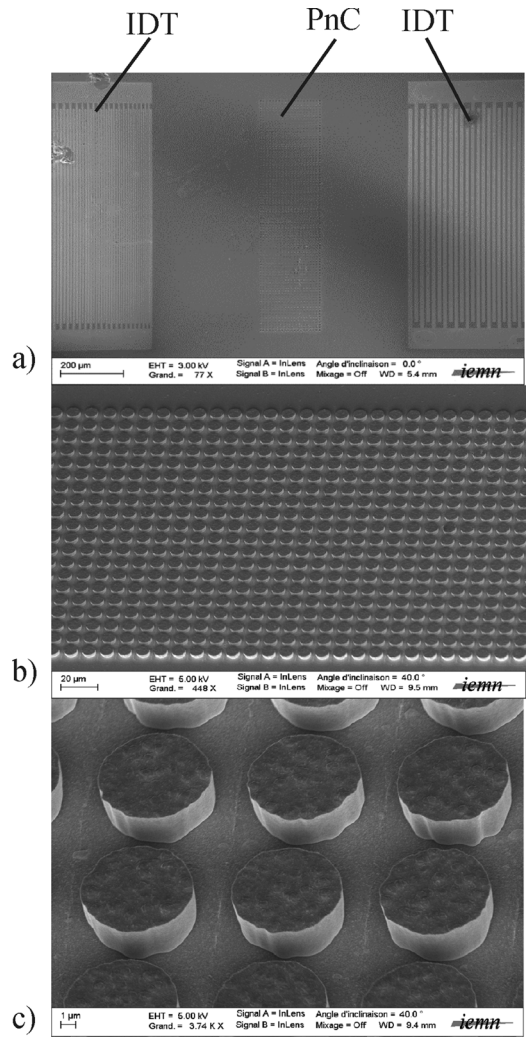

FIG. 7. Scanning electron microscopy image of one of the fabricated PnC structure with $a = 10\,\mu$m, $r = 3.8\,\mu$m, and $h = 3.4\,\mu$m: (a) complete device (IDTs and PnC); (b) zoom on the PnC; and (c) zoom on the pillars.

calibration, we eliminate the effect of electromagnetic crosstalk and fast bulk acoustic waves by using the time gating capability of the network analyzer. Treated results in form of $\Delta S_{21\,\mathrm{exp}}$ and $\Delta\varphi_{\mathrm{exp}}$ are shown on Fig. 8. For comparison, the theoretical results obtained by numerical simulation are also depicted on the same figure (dashed line). The normalized transmission responses are shown in Figs. 8(a) and 8(c) for two configurations corresponding to pillars thickness close to 2.3 and to 3.4 μm, respectively. We observed that the measured first stop-band, corresponding to the local resonance mode in pillars, agrees quite well with the frequency range band gap obtained by FE calculations. However, the second band gap is shifted by about 10–15 MHz for the two configurations. A possible explanation of this shift is the difference between the elastic properties of the pillar material used in the calculations and the actual values of the density and elastic constants of deposited nickel. Some additional frequency shift for the second set of parameters is due to the fact that the radius of fabricated pillars was slightly smaller than 3.8 μm. Nevertheless, the remaining part of the experimental curves accurately coincides with the theoretical ones.

It should be noted that the phase clearly indicates the location of the band-gaps which are mainly characterized by flat band.

V. CONCLUSIONS

In this paper, interaction of surface acoustic wave with 2D PnC on a piezoelectric substrate was explored both theoretically and experimentally. Both analyses were successfully conducted for PnCs with various thicknesses. It was demonstrated that pillar's height increase leads to a reduction of the center frequency for the first local resonance band gap and to formation of the second Bragg gap and the propagation zone between them. Quantitative characteristics of SAW attenuation inside observed bandgaps were obtained

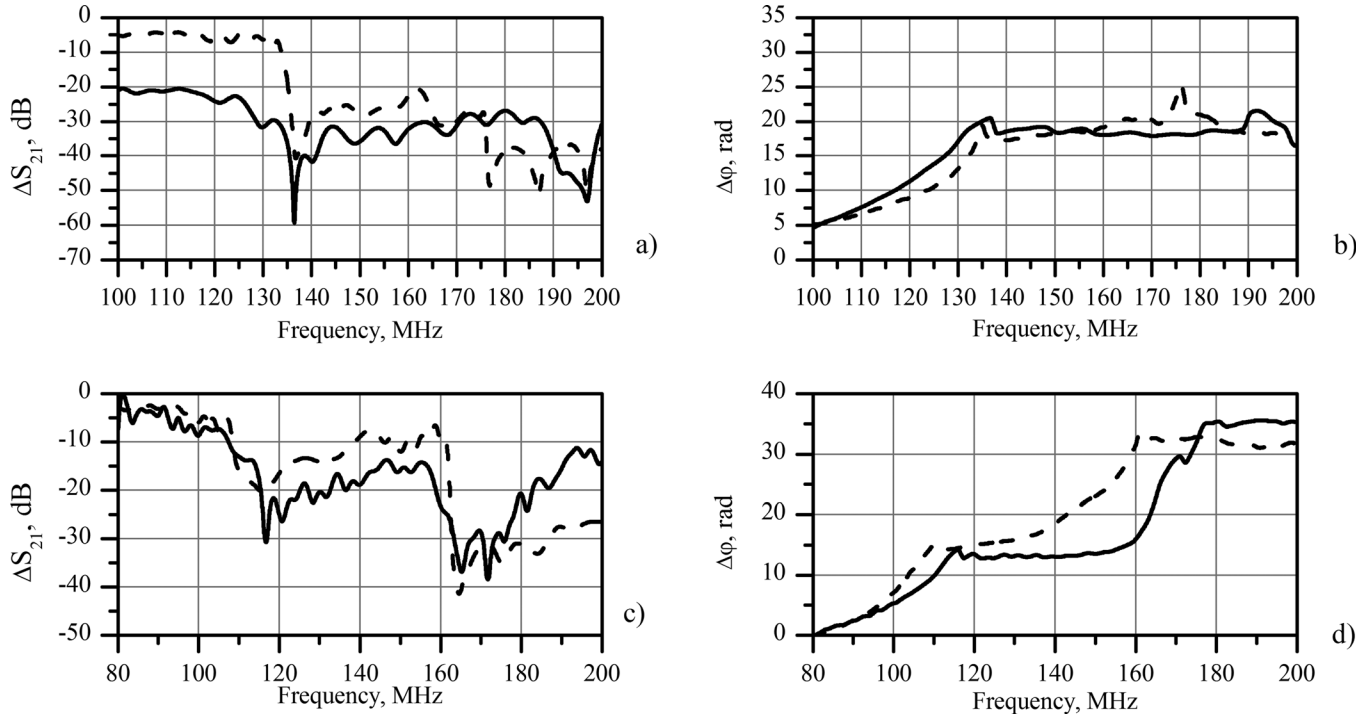

FIG. 8. Frequency dependence of relative transmission ΔS_{21} (a) and (c), and phase difference $\Delta\varphi_{exp}$ (b) and (d) measured experimentally (solid line) and obtained by FE calculations (dashed line) for pillar height $h = 2.3\ \mu$m (a) and (b), and $h = 3.4\ \mu$m (c) and (d).

via suggested model for transmission calculation. Furthermore, it was shown that slope change on the phase difference frequency dependence defines the beginning of local resonance, and constant phase difference corresponds to forbidden zone for SAW. Moreover, the similar slope change exists for Bragg bandgap. Fairly good experimental confirmation of SAW propagation characteristics was achieved through direct scattering matrix measurements of fabricated test dispersive delay lines with observed phononic crystal arrays.

The described model is applicable to different PnC structures on piezoelectric substrates. Owing to the ferromagnetic properties of Nickel, further investigations can also be performed incorporating magneto-elastic coupling in PnCs[10] to develop a sensitive magnetic sensor.

ACKNOWLEDGMENTS

This work was supported by the following Grants Nos. 11.G34.31.0030 (the Government of the Russian Federation), ANR-12-BS09-0015-01 (The French National Research Agency) and co-joint PhD scholarship grant of the French Ministry of Foreign Affairs (French Embassy in Russian Federation).

[1]P. Deymier, *Acoustic Metamaterials and Phononic Crystals*, Springer Series in Solid-State Sciences Vol. 173, edited by P. Deymier (Springer-Verlag, Berlin-Hidelberg, 2013) available at http://link.springer.com/book/10.1007%2F978-3-642-31232-8.
[2]Y. Pennec, J. O. Vasseur, B. Djafari-Rouhani, L. Dobrzyński, and P. A. Deymier, Surf. Sci. Rep. **65**, 229 (2010).
[3]M. Sigalas and E. N. Economou, Solid State Commun. **86**, 141 (1993).
[4]Y. Tanaka and S. Tamura, Phys. Rev. B **58**, 7958 (1998).
[5]J. H. Page, P. Sheng, H. P. Schriemer, I. P. Jones, X. D. Jing, and D. A. Weitz, Science **271**, 634 (1996).
[6]M. Torres and F. R. Montero de Espinosa, Ultrasonics **42**, 787 (2004).
[7]A. M. Kosevich, JETP Lett. **74**, 559 (2001).
[8]R. James, S. M. Woodley, C. M. Dyer, and V. F. Humphrey, J. Acoust. Soc. Am. **97**, 2041 (1995).
[9]M. M. de Lima, Jr., R. Hey, P. V. Santos, and A. Cantarero, Phys. Rev. Lett. **94**, 126805 (2005).
[10]O. Bou Matar, J. F. Robillard, J. O. Vasseur, A.-C. Hladky-Hennion, P. A. Deymier, P. Pernod, and V. Preobrazhensky, J. Appl. Phys. **111**, 054901 (2012).
[11]S. Mohammadi, A. A. Eftekhar, W. D. Hunt, and A. Adibi, Appl. Phys. Lett. **94**, 051906 (2009).
[12]V. Laude, A. Khelif, T. Pastureaud, and S. Ballandras, J. Appl. Phys. **90**, 2492 (2001).
[13]A. Khelif, A. Choujaa, S. Benchabane, B. Djafari-Rouhani, and V. Laude, Z. Kristallogr. **220**, 836 (2005).
[14]J. H. Page, S. Yang, Z. Y. Liu, M. L. Cowan, C. T. Chan, and P. Sheng, Z. Kristallogr. **220**, 859 (2005).
[15]V. Laude, L. Robert, W. Daniau, A. Khelif, and S. Ballandras, Appl. Phys. Lett. **89**, 083515 (2006).
[16]J. O. Vasseur, A.-C. Hladky-Hennion, B. Djafari-Rouhani, F. Duval, B. Dubus, and Y. Pennec, J. Appl. Phys. **101**, 114904 (2007).
[17]T.-T. Wu, Z.-G. Huang, T.-C. Tsai, and T.-C. Wu, Appl. Phys. Lett. **93**, 111902 (2008).
[18]Y. Pennec, B. Djafari-Rouhani, H. Larabi, J. O. Vasseur, and A. C. Hladky-Hennion, Phys. Rev. B **78**, 104105 (2008).
[19]T.-C. Wu, T.-T. Wu, and J.-C. Hsu, Phys. Rev. B **79**, 104306 (2009).
[20]V. Laude, M. Wilm, S. Benchabane, and A. Khelif, Phys. Rev. E **71**, 036607 (2005).
[21]S. Benchabane, A. Khelif, J.-Y. Rauch, L. Robert, and V. Laude, Phys. Rev. E **73**, 065601 (2006).
[22]A. Khelif, Y. Achaoui, S. Benchabane, V. Laude, and A. Boujemaa, Phys. Rev. B **81**, 214303 (2010).
[23]Y. Achaoui, A. Khelif, S. Benchabane, L. Robert, and V. Laude, Phys. Rev. B **83**, 104201 (2011).
[24]A. Talbi, Y. Du, S. Yankin, J. Streque, J.-C. Gerbedoen, A. Mrabti, A. Akjouj, Y. Pennec, B. Djafari Rouhani, P. Pernod, V. Preobrazhensky, O. Bou Matar, and H. Tang, in *Proceedings of 2013 IEEE International Ultrasonics Symposium (IUS), Prague, Czech Republic, 21–25 July 2013* (IEEE, 2013), p. 2130.
[25]T.-T. Wu, L.-C. Wu, and Z.-G. Huang, J. Appl. Phys. **97**, 094916 (2005).
[26]D. W. Dissanayake, *Acoustic Waves* (Sciyo Publishing, Croatia, 2010).

[27]T.-T. Wu, W.-S. Wang, J.-H. Sun, J.-C. Hsu, and Y.-Y. Chen, Appl. Phys. Lett. **94**, 101913 (2009).
[28]S. Hemon, A. Akjouj, A. Soltani, Y. Pennec, Y. El Hassouani, A. Talbi, V. Mortet, and B. Djafari-Rouhani, Appl. Phys. Lett. **104**, 063101 (2014).
[29]S. A. Nikitov, A. V. Grigor'evskii, V. I. Grigor'evskii, I. M. Kotelyanskii, V. A. Luzanov, E. N. Mirgorodskaya, and S. G. Suchkov, J. Commun. Technol. Electr. **56**, 888 (2011).
[30]COMSOL Multiphysics 4.3a, www.comsol.com (2013).
[31]D. Morgan, *Surface Acoustic Wave Filters* (Academic, London, 2007).